



Streak creation using groove and heating patterns

S. Panday * and J. M. Floryan *Department of Mechanical and Materials Engineering, The University of Western Ontario, London, Ontario, Canada N6A 5B9*

(Received 17 April 2022; accepted 22 July 2022; published 5 August 2022)

The use of streamwise grooves for intensification of streaks created by heating in shear layers has been investigated. Three ranges of groove wave numbers were of interest: wave numbers near the critical wave number of the Rayleigh-Bénard (RB) instability, wave numbers characterizing drag-reducing grooves, and the optimal wave numbers. It is shown that uniform heating of a grooved surface produces intense streaks only when the groove wave number is near the critical RB wave number and the heating intensity exceeds the critical RB intensity. The use of long-wavelength grooves reduces flow losses, but the resulting streaks are less intense. The use of heating patterns tuned with groove patterns can produce very intense streaks whose spatial distribution is easily controlled through selection of the patterns' wave number. An increase of flow losses due to patterned heating can be compensated for using spatial groove distributions with drag-reducing capabilities. It has been demonstrated that the most effective wave number producing high-intensity streaks at low flow losses is between the RB wave number and the drag-reducing wave numbers—this optimal wave number has been identified.

DOI: [10.1103/PhysRevFluids.7.083502](https://doi.org/10.1103/PhysRevFluids.7.083502)

I. INTRODUCTION

Mixing is a process of importance in geophysics, astrophysics, engineering, physiology, and other areas [1–4] but difficult to achieve in low Reynolds number flows [5–8]. It is known that rolls and streaks play significant roles in shear layer instabilities and the transition to turbulence [9–14] and thus could be utilized for mixing intensification. The natural formation of streaks generally takes place in high Reynolds number flows indicating that an external forcing may be required to generate streaks in low Reynolds number laminar flows. Various types of forcing schemes for active stirring are discussed in [15].

Rolls are vortices in the flow cross-plane which transport high-speed fluid towards the wall (downwash) and low-speed fluid away from the wall (upwash), thereby creating streaks in the main flow velocity field [16]. These streaks are themselves subject to instabilities [14] which may lead to optimal roll structures that maximize the transient temporal growth of streaks [17] or to the growth of the normal modes leading to secondary instabilities [16]. The primary role of streaks in mixing processes is either to induce known instabilities or to create new instabilities leading to saturation states with desired properties.

Most of the existing studies are focused on naturally occurring rolls, which limits their use to large-Re flows and does not provide the means for controlling their structure. Rolls with a specific structure can be created by bypassing instability processes using various surface modifications but at a significant “cost” measured in terms of pressure losses [5–7,18]. The search for suitable methods for the formation of rolls at small Reynolds numbers, with minimal pressure losses

*spanday2@uwo.ca

and with a desired spatial structure, started very recently [19]. It is known that streaks can be created using longitudinal grooves—these streaks activate an instability mode [20,21] which leads to a saturation state producing chaotic stirring at small Reynolds numbers [22]. Remarkably, the associated pressure losses decrease compared to a smooth channel [23]. We acknowledge that there are other surface topographies capable of producing streaks [24] and chaotic mixing [25] but there is not much information in the literature about the associated pressure losses.

This paper is focused on the analysis of the use of heating for streak formation. It is known that uniform heating leads to natural convection in the form of Rayleigh-Bénard (RB) rolls [26,27] with the RB instability dictating the form of these rolls in fully developed shear layers [28]. Uniform heating can also be used to create rolls in developing shear layers [29–33] with their structure dictated by the critical disturbance wave number. To move away from this restriction, patterned heating was introduced—this heating created a horizontal field of buoyancy forces with the desired spatial distribution and was quite effective in creating well-controlled rolls [19]. The rolls were driven by horizontal temperature gradients and occurred regardless of the heating intensity—such rolls represent a forced response rather than a bifurcation as is the case of rolls created by RB convection. While our focus is on heating, we acknowledge that other natural instabilities can be used for roll formation [34,35] but the spatial structure of such rolls is always determined by the critical wave number at the onset of instability.

Heating patterns produce weak modifications of the velocity field which are significant in the spanwise cross section but marginal in the streamwise direction [36,37], and are sensitive to the fluid Prandtl number [38]. Because of that, it is preferable to consider streamwise and spanwise heating patterns separately as they activate different physical mechanisms. The streamwise patterns do not produce streaks but are known to reduce pressure losses at small Reynolds numbers [39,40] and to decrease the flow resistance in the relative movement of plates [41]. The spanwise patterns are known to produce streaks [19]. This analysis is therefore focused on the use of spanwise heating patterns.

The starting point is the creation of streaks using different heating methods applied to smooth surfaces [19]. We wish to explore if the addition of grooves can result in more intense streaks as well as to determine the effect of heated grooves on flow losses. Grooves by themselves create flow modifications which lead to chaotic mixing [22]. Long-wavelength grooves reduce pressure losses [23]. The addition of heating to grooved surfaces may produce intense streaks at negligible pressure losses. We are interested in small heating rates to reduce the energy cost; i.e., the relevant Rayleigh numbers Ra are small. Large Ra convection is of no interest to this analysis—a recent review of such convection over rough surfaces can be found in [42]. Streaks produce spanwise gradients of the streamwise velocity component which are known to give rise to secondary flows driven by an inviscid instability mechanism [20] leading to chaotic mixing [22]. This analysis can be viewed as a step in the evaluation of potential heating patterns for creation of chaotic mixing; i.e., it deals with determination of the primary state involving streaks which will be subsequently subject to stability analysis.

Our presentation is organized as follows. Sec. II describes our model problem—flow in a channel equipped with longitudinal grooves and exposed to a combination of uniform and spanwise-periodic heating. In Sec. III we characterize streaks created by uniform heating of a grooved wall. In Sec. IV we describe streaks created by spanwise-periodic heating of grooves. In Sec. V we describe streaks created by a combination of uniform and periodic heating of grooved surfaces. In Sec. VI we provide a short summary of the main conclusions.

II. PROBLEM FORMULATION

Consider flow in a channel formed by two horizontal plates extending to $\pm\infty$ in the x and z directions (see Fig. 1), with the lower wall being equipped with longitudinal grooves and the upper wall being smooth, and with gravity acting in the negative y direction. The mean distance between

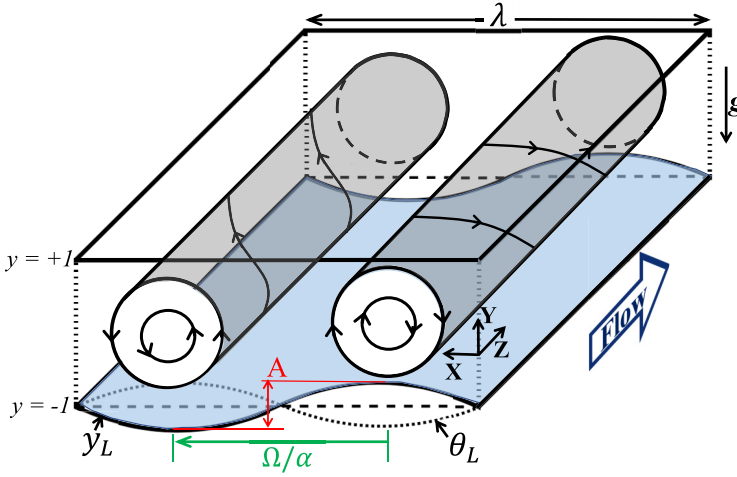


FIG. 1. Schematic diagram of the flow configuration.

the walls is $2h^*$. The geometry of the channel is given as

$$y_U = 1, \quad y_L(x) = -1 + \frac{A}{2} \cos(\alpha x). \quad (1)$$

where subscripts L , U refer to the lower and upper walls, respectively; A stands for the groove amplitude; α denotes the wave number; the symbol $\lambda = 2\pi/\alpha$ is used to denote wavelength; h^* is used as the length scale; and stars denote dimensional quantities.

The upper wall is isothermal while the lower wall is heated with temperature variations being at most of $O(10)$ which leads to acceptability of the Boussinesq fluid model [43]. The fluid has thermal conductivity k^* , specific heat c^* , thermal diffusivity $\kappa^* = k^*/\rho^*c^*$, kinematic viscosity ν^* , dynamic viscosity μ^* , and thermal expansion coefficient Γ^* and it is driven in the positive z direction by a fixed pressure gradient. The relative wall temperatures are

$$\theta_U = 0, \quad \theta_L(x) = \text{Ra}_{\text{uni}} + \frac{\text{Ra}_P}{2} \cos(\alpha x + \Omega), \quad (2)$$

where $\theta = T - T_U$ is the relative temperature with respect to the temperature of the upper wall, T stands for the absolute temperature, $\kappa^*\nu^*/(g^*\Gamma^*h^{*3})$ is the temperature scale, the uniform Rayleigh number $\text{Ra}_{\text{uni}} = g^*\Gamma^*h^{*3}\theta_{\text{uni}}^*/(\kappa^*\nu^*)$ determines the intensity of the uniform component of heating, the periodic Rayleigh number $\text{Ra}_P = g^*\Gamma^*h^{*3}\theta_{LP}^*/(\kappa^*\nu^*)$ determines the intensity of the periodic heating component, and Ω is the phase shift between the topography and temperature patterns. The groove and temperature patterns are perfectly tuned; i.e., they are described by the same wave number, with the pattern interaction effect being driven by spatial positioning of these patterns.

Formation of rolls and streaks is described by the continuity, Navier-Stokes, and energy equations of the form

$$\frac{\partial u}{\partial x} + \frac{\partial v}{\partial y} + \frac{\partial w}{\partial z} = 0, \quad (3a)$$

$$u \frac{\partial u}{\partial x} + v \frac{\partial u}{\partial y} + w \frac{\partial u}{\partial z} = -\frac{\partial p}{\partial x} + \nabla^2 u, \quad (3b)$$

$$u \frac{\partial v}{\partial x} + v \frac{\partial v}{\partial y} + w \frac{\partial v}{\partial z} = -\frac{\partial p}{\partial y} + \nabla^2 v + \text{Pr}^{-1} \theta \quad (3c)$$

$$u \frac{\partial w}{\partial x} + v \frac{\partial w}{\partial y} + w \frac{\partial w}{\partial z} = -\frac{\partial p}{\partial z} + \nabla^2 w, \quad (3d)$$

$$u \frac{\partial \theta}{\partial x} + v \frac{\partial \theta}{\partial y} + w \frac{\partial \theta}{\partial z} = \text{Pr}^{-1} \nabla^2 \theta, \quad (3e)$$

where $U_v^* = v^*/h^*$ is the velocity scale, $\rho^* U_v^{*2}$ is the pressure scale, and $\text{Pr} = \nu^*/\kappa^*$ is the Prandtl number. The relevant boundary conditions are

$$u = v = w = 0 \text{ at } y = y_L \text{ and } y = 1, \quad (4a)$$

$$\theta(x, y_L, z) = \theta_L(x), \quad \theta(x, 1, z) = 0. \quad (4b)$$

The geometry and heating conditions result in $\frac{\partial}{\partial z} = 0$, thus decoupling (3a)–3(c) and 3(e) from (3d)—this leads to a two-step solution process starting with solution of the nonlinear problem (3a)–3(c) and 3(e) followed by solution of a linear problem (3d). The linearity of (3d) permits the elimination of Re as a parameter through a simple scaling. The cost of streak formation is quantified by comparing properties of flow in the z direction with the isothermal form of this flow in a smooth channel. This reference flow has the following form:

$$\bar{u}_0(x, y, z) = [0, 0, w_0] = [0, 0, \text{Re}(1 - y^2)], \quad p_0(x, y, z) = -2z \text{Re}, \quad Q_0 = \frac{4}{3} \text{Re}. \quad (5)$$

In the above, subscript 0 denotes the isothermal quantities and the Reynolds number is defined as $\text{Re} = W_{\max}^* h^* / \nu^* = W_{\max}^* / U_v^*$ where W_{\max}^* denotes the maximum of the z -velocity component.

We use two methods of assessing the cost of the streaks' creation. In the first one, we assume that the pressure gradient in the z direction remains the same with and without heating and grooves; i.e., we impose the fixed pressure gradient constraint of the form

$$\frac{\partial p}{\partial z} \Big|_{\text{mean}} = -2\text{Re}, \quad (6)$$

and determine change of the flow rate Q_c , i.e.,

$$Q_c = Q - Q_0, \quad Q = \lambda^{-1} \int_0^\lambda \int_{y_L}^{+1} w \, dy dx, \quad (7)$$

where positive Q_c corresponds to an increase of the flow rate. Alternatively, we impose the fixed flow rate constraint of the form

$$Q = \frac{4}{3} \text{Re}, \quad (8)$$

and determine the reduction of the required pressure gradient P_c , i.e.,

$$P_c = \frac{\partial p}{\partial z} \Big|_{\text{mean}} - \frac{dp_0}{dz}, \quad (9)$$

with the positive P_c corresponding to the reduction of pressure losses. We eliminate any external forces which might drive the flow in the x direction by imposing the zero mean pressure gradient constraint of the form

$$\frac{\partial p}{\partial x} \Big|_{\text{mean}} = 0. \quad (10)$$

System (3)–(10) is solved numerically using spectrally accurate discretization relying on Fourier expansions in the horizontal directions and Chebyshev expansions in the transverse direction. The main challenge is posed by the irregularity of the solution domain dictated by the groove geometry. The challenge becomes more pronounced by the need to consider a wide range of geometries resulting from variations of the groove wave number and amplitude. This problem was handled using a concept known as the immersed boundary conditions (IBC) method. This strategy uses the fixed computational domain, while the specific flow domain is immersed inside this computational

domain. The discretized flow equations remain unchanged across all geometries and are solved simultaneously both inside and outside of the flow domain, but always inside the computational region. It is ensured that the flow boundaries are located inside the computational domain and the flow conditions at these boundaries are posed as constraints [44–46]. The Tau method has been implemented in order to incorporate boundary conditions into the coefficient matrix. This formulation avoids the need for the numerical construction of intricate grids that replicate the groove geometry, which can be very labor intensive and error prone, and circumvents the need for grid convergence studies. All the elements of the discretization have spectral accuracy. The global accuracy of the algorithm is controlled by changing the number of Fourier modes and Chebyshev polynomials—all results presented in this paper were obtained with an accuracy of at least four digits. The groove shape is encoded within the algorithm by means of appropriate Fourier expansions, which means that variations of groove geometry can be accounted for by simply changing the Fourier coefficients. Alternative methods for handling the irregularity of the flow domain are discussed by Cabal *et al.* [47]. Detailed implementation of the algorithm developed for this study can be found in [48].

It is of interest to monitor the change in heat fluxes owing to the use of grooves. These fluxes are presented in terms of the Nusselt number correction Nu_c . This correction has been determined by evaluating the Nusselt number Nu for the grooved channel and then subtracting the Nusselt number associated with conduction in a smooth channel Nu_{cond} from it, i.e.,

$$Nu_c = Nu - Nu_{\text{cond}}, \quad Nu_{\text{cond}} = \frac{1}{2}Ra_{\text{uni}}. \quad (11)$$

Positive Nu_c corresponds to an increase of the heat flow. Our interest is in creation of strong streaks while minimizing cost expressed either in terms of pressure losses or in terms of flow losses. We shall explore three strategies: (i) use of the uniform heating of grooved surfaces, (ii) spanwise-periodic heating of grooved surfaces, and (iii) use of a combination of uniform and periodic heating of grooved surfaces. We note that the spatial distribution of streaks is dictated by the groove and heating patterns.

III. UNIFORM HEATING—ISOTHERMAL GROOVES

Both walls are isothermal with the temperature of the lower wall being higher than the temperature of the upper wall. Uniform Rayleigh number Ra_{uni} measures the temperature difference between these walls. Two ranges of groove wave numbers are of interest for uniform heating: (i) the long-wavelength grooves which are known to reduce flow losses [23,49], and (ii) grooves with $\alpha \approx 1.57$ which is the critical wave number for the Rayleigh–Bénard (RB) instability [26,27]. The former one is of interest as it implies lower flow losses associated with formation of streaks. The latter one is of interest as it takes advantage of the RB instability to increase streak intensity—the heating intensity must, however, reach the critical value ($Ra_{\text{uni}} = 213.5$) required for the instability onset. We shall refer to the latter range of wave numbers as the RB range. Flow topology, which can be created using isothermal grooves in the latter case, is illustrated in Fig. 2. Temperature contours indicate the presence of the x -temperature gradients, which generate transverse movement [50,51] resulting in the formation of rolls and streaks. Particle trajectories illustrate rolling up the fluid layers in spirals. The spiral movement allows stretching of the fluid layers which is a characteristic feature for chaotic mixing [22]. Topologies for the small- α streaks are similar and thus are not shown.

The strength of the streaks is measured in two ways: (i) using change of the fluid kinetic energy,

$$\Delta E_k = E_k - E_{k,0} = \lambda^{-1} \int_0^\lambda \int_{y_L}^{+1} (u^2 + v^2 + w^2) dy dx - \int_{-1}^{+1} w_0^2 dy, \quad (12)$$

and (ii) using the maximum of the spanwise gradient of the longitudinal velocity component,

$$\xi = \max\left(\frac{dw}{dx}/\text{Re}\right), \quad (13)$$

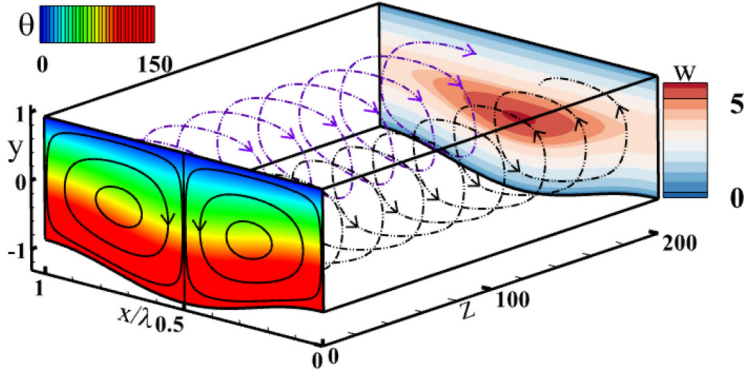


FIG. 2. Flow topology in an isothermal grooved channel for $\alpha = 1.57$, $A = 0.4$, $Ra_{uni} = 150$, $Ra_{P,L} = 0$, and $Pr = 0.71$. Colors in the front (x, y) plane illustrate the temperature field while the black solid line illustrates vector lines, colors in the rear (x, y) plane represent the w -velocity field, and dash-dotted lines show particle trajectories.

in the midsection of the channel. The latter one is of interest as such shear is responsible for flow instabilities leading to chaos [22]. In the above, E_k stands for the kinetic energy of the actual flow while $E_{k,0}$ stands for the kinetic energy of the reference flow. Variations of ΔE_k displayed in Fig. 3(a) for $\alpha = 1.57$ demonstrate fairly weak streaks for small Ra'_{uni} s. Their intensity rapidly increases when Ra_{uni} approaches the critical value of 213.5 with grooves of higher amplitude producing stronger streaks. Variations of ξ displayed in Fig. 3(b) illustrate the effect of the RB mechanism on the intensification of streaks for α near $\alpha = 1.57$ for a sufficiently large Ra_{uni} . Reduction of ξ at large α 's is associated with formation of a convection boundary layer near the grooved wall while ξ is evaluated in the channel midsection. Reduction of ξ at small α 's is due to the reduction of horizontal x -temperature gradients. The reference results for the isothermal grooved channel and uniformly heated smooth channel demonstrate the large advantage offered by uniformly heated grooves.

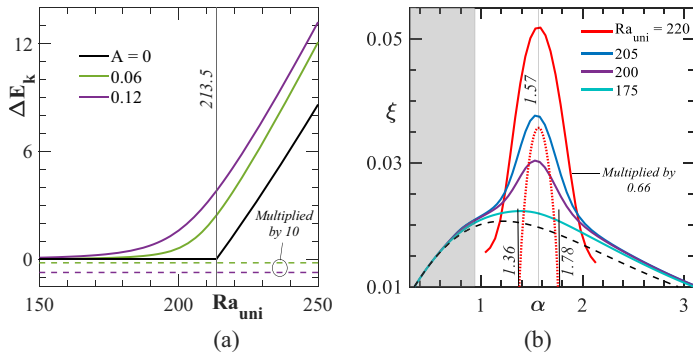


FIG. 3. (a) Variations of the change in kinetic energy ΔE_k [Eq. (12)] as a function of Ra_{uni} for $\alpha = 1.57$, $Ra_{P,L} = 0$, $Re = 5$ and selected A 's. (b) Variation of the maximum of the spanwise velocity gradient ξ [Eq. (13)] as a function of α for $A = 0.06$, $Ra_{P,L} = 0$, and selected Ra'_{uni} s. Dashed lines provide results for isothermal grooved channel. Red dotted line in (b) shows results for a smooth channel with $Ra_{P,L} = 220$. Gray color identifies α 's leading to a reduction of pressure losses in a grooved isothermal channel.

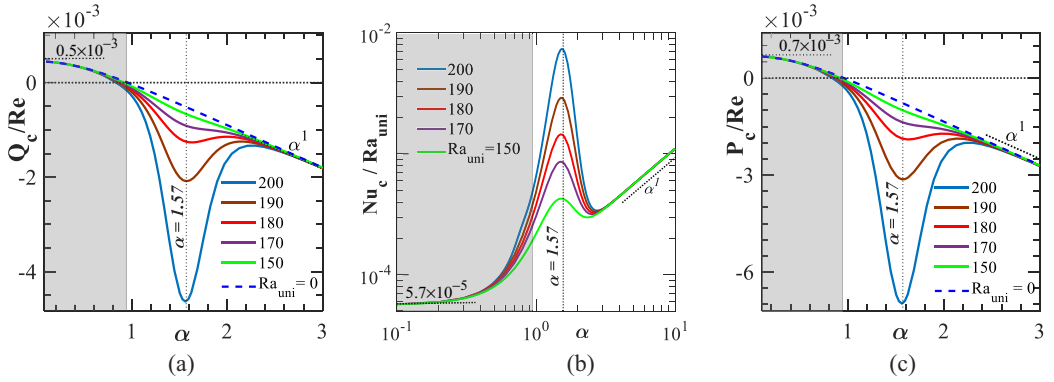


FIG. 4. Variation of the flow rate correction Q_c [Eq. (7)] (a), the Nusselt number correction Nu_c [Eq. (11)] (b), and the pressure gradient correction P_c [Eq. (9)] (c) as functions of α for $A = 0.06$ and $Ra_{P,L} = 0$. The dashed lines in (a,c) correspond to the isothermal grooved channel; gray shading identifies α 's leading to a reduction of pressure losses (increase of the flow rate) in such channel.

Formation of streaks increases flow losses as illustrated in Fig. 4—reduction of the flow rate is illustrated in Fig. 4(a) while increase of the pressure gradient is illustrated in Fig. 4(c)—these data measure the energy cost associated with streak creation. Heating increases losses over the whole range of α 's with a local peak forming for $\alpha \approx 1.57$. Figure 4(b) illustrates the heat transfer consequences of streak formation. The region shaded in gray identifies conditions where introduction of unheated grooves reduces flow losses. Addition of heating marginally increases losses for such α 's. It is possible to use such heated grooves for streak creation without paying a penalty in the form of increased losses—the overall energy cost of flows with streaks is still below the energy cost of flow without heating and grooves.

Data displayed in Fig. 5 demonstrate increase of the effectiveness of streak formation for larger groove amplitudes for both the drag-reducing α 's as well as for α 's in the RB zone. The energy cost of using α 's in the RB zone monotonically increases with A while use of α 's in the drag-reducing zone initially reduces losses but its excessive increase reverses this trend, and the losses begin to increase rapidly.

Streaks are used to create spanwise shear layers which are expected to trigger a unique kind of instability [20,21] which is the initial step towards chaotic stirring [22]. The spanwise distributions

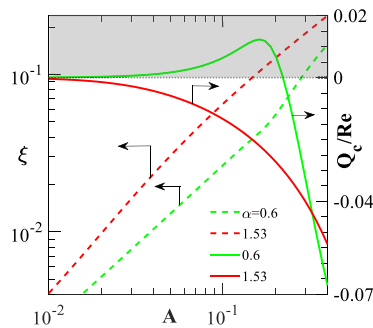


FIG. 5. Variations of the maximum of the spanwise velocity gradient ξ [Eq. (13), dashed lines] and the flow rate correction Q_c [Eq. (7), solid lines] as functions of the groove amplitude A for $\alpha = 0.6$ (green lines, the drag-reduction zone) and $\alpha = 1.53$ (red lines, the RB zone) for $Ra_{umi} = 205$, $Ra_{P,L} = 0$. Gray shading identifies conditions leading to an increase of the flow rate.

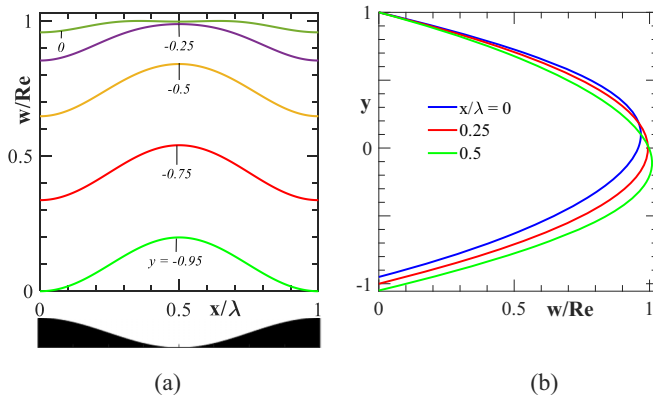


FIG. 6. Spanwise distributions of the w -velocity component at different y locations (a) and the transverse distributions of the w -velocity component at different x locations (b) for $\alpha = 1.57$, $Ra_{uni} = 200$, $Ra_{P,L} = 0$, $A = 0.1$.

of the streamwise velocity component are displayed in Fig. 6(a) for α in the RB zone. They demonstrate velocity increase near the groove trough and reduction around the groove crest resulting in the formation of transverse shear layers. The spanwise gradients of the w -velocity component decrease with distance away from the grooved wall—these gradients are responsible for activation of the inviscid instability mechanism described in [20]. The wall-normal distributions of the w -velocity component displayed in Fig. 6(b) demonstrate small changes in vertical shear concentrated close to the grooved wall. They produce a minor modification of the classical shear-driven instability [21]. Plots of the w -velocity component for α 's in the loss reduction zone have a qualitatively similar form and thus are not shown. The spanwise velocity gradient for such α 's is much smaller, but this can be compensated for by using larger groove amplitudes (see Fig. 5).

IV. PERIODIC HEATING AND PATTERN INTERACTION EFFECT

The presence of grooves creates spanwise modulations in the flow and its uniform heating produces streaks with the pattern dictated by the groove wave number. In this section we investigate the use of periodic heating of a grooved surface which provides the means for creation of potentially stronger streaks [19]. We focus attention on heating patterns perfectly tuned with the groove patterns where both effects can potentially reinforce each other. The presence of patterns of distinct physical quantities activates the pattern interaction effect [52] which may either weaken or amplify the streak formation process. In this case, the interaction of groove and heating patterns creates net spanwise flow which may be directed either to the left or to the right depending on the relative positions of both patterns.

The relative position of both patterns is measured using phase difference Ω with $\Omega = 0$ corresponding to hot spots overlapping with the groove crests and $\Omega = \pi$ corresponding to hot spots overlapping with groove troughs—the pattern interaction effect is not active for these two special configurations [52]. Results displayed in Fig. 7(a) demonstrate that the strongest streaks are obtained for the hot spots placed halfway between the groove crests and troughs for low heating, i.e., $Ra_{P,L} = 200$. Increase of heating to $Ra_{P,L} = 400$ shows a preference for placing hot spots closer to the groove trough for $\alpha = 0.6$ (drag-reducing zone) and $\alpha = 1$ but retains the previous preference for $\alpha = 1.57$ (RB zone). Use of $\alpha \approx 1$ leads to the strongest streaks so $\alpha = 1$ is viewed as optimal and is added to the further discussion of potential gains due to periodic heating of grooved walls. Distributions of ξ displayed in Fig. 7(b) lead to somewhat different conclusions as all α 's show preference for placing hot spots approximately halfway between the groove crests and troughs. Addition of grooves to a periodically heated wall increases flow losses for α 's in the RB zone and

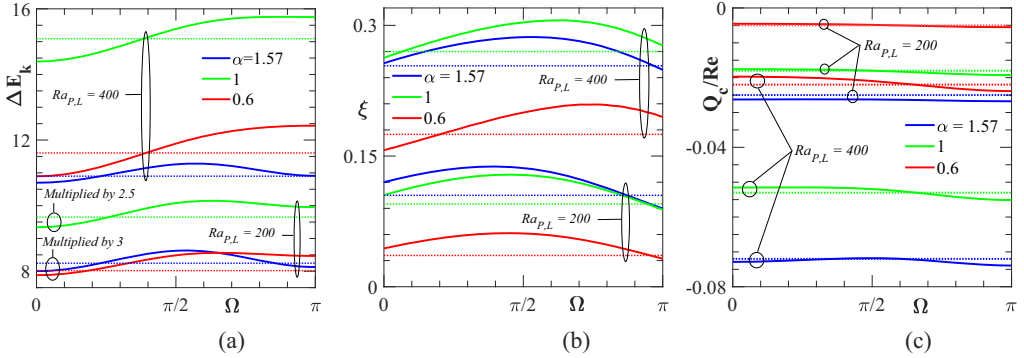


FIG. 7. Variations of the change in kinetic energy ΔE_k [Eq. (12)] (a), the maximum of the spanwise velocity gradient ξ [Eq. (13)] (b), and the flow rate correction Q_c [Eq. (7)] (c) as functions of Ω for $\alpha = 1.57$ (the RB zone, solid blue lines), $\alpha = 1$ (solid green lines), and $\alpha = 0.6$ (the drag-reduction zone, solid red lines), $Ra_{uni} = 0$, $A = 0.1$, and $Ra_{p,L}$ s are specified in the figures. Reference quantities for a smooth channel exposed to the same periodic heating are illustrated using dotted lines. The reference quantities for a grooved isothermal channel are $\alpha = 1.57$: $\Delta E_k = -0.0515$, $\xi = 0.0326$, $Q_c/Re = -0.0014$; $\alpha = 1$: $\Delta E_k = 0.0095$, $\xi = 0.0334$, $Q_c/Re = -0.0001$; $\alpha = 0.6$: $\Delta E_k = 0.0507$, $\xi = 0.0259$, $Q_c/Re = 0.0007$.

can decrease losses for $\alpha = 0.6$ (drag-reducing zone) and $\alpha = 1$ depending on Ω as illustrated in Fig. 7(c).

The above discussion shows that the configuration of interest is $\alpha = 1$ as it generates very strong streaks without paying an excessive penalty in terms of flow losses. The reader may note that positioning of hot spots halfway between the groove crests and troughs, which is the most effective configuration at small heating rates, results in the strongest thermal drift [51,53]. The overall flow topology for such conditions is presented in Fig. 8, showing net flow to the left.

Results displayed in Fig. 9 permit assessment of effects of the pattern wave numbers and identification of the most effective α . Variations of ΔE_k displayed in Fig. 9(a) demonstrate that streak intensity changes significantly as a function of α with $\alpha \approx 1$ being the most effective, regardless if the smooth or grooved heated surfaces are used. Use of a grooved isothermal channel produces an order of magnitude weaker streaks while use of a heated smooth channel produces competitive streaks, but weaker than those obtained with a heated grooved channel with a proper

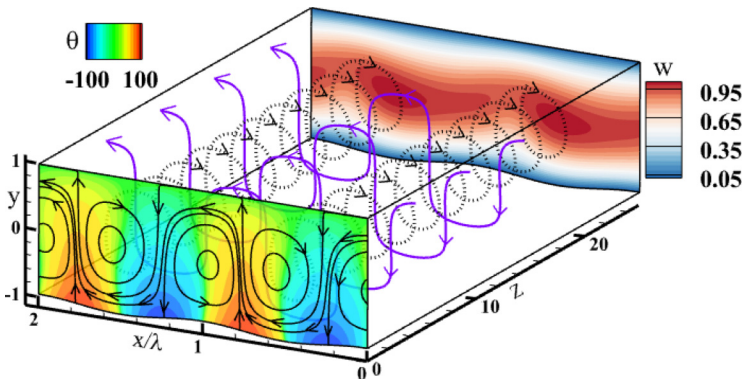


FIG. 8. Topology of flow in an isothermal grooved channel for $\alpha = 1$, $A = 0.1$, $Ra_{uni} = 0$, $Ra_{p,L} = 200$, $\Omega = \pi/2$, and $Re = 1$. Colors in the front (x, y) plane illustrate the temperature field while the black solid line illustrates velocity vector lines, and colors in the rear (x, y) plane represent the w -velocity field. Black dotted and purple solid lines inside the plotted box show particle trajectories.

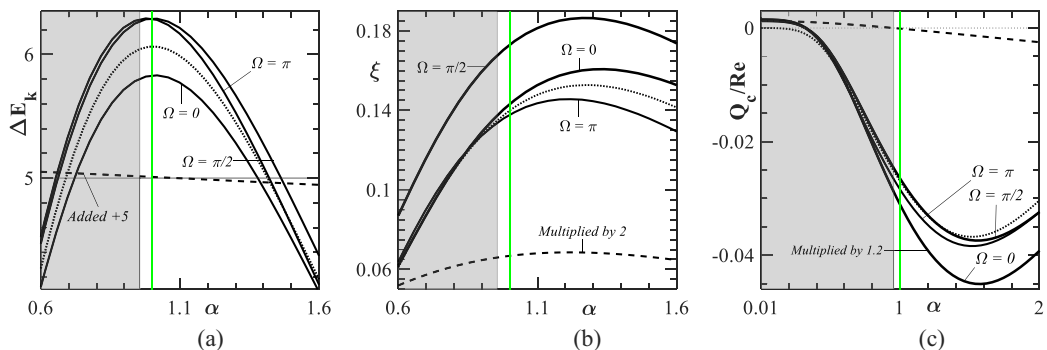


FIG. 9. Variations of the change in kinetic energy ΔE_k [Eq. (12)] (a), the maximum of the spanwise velocity gradient ξ [Eq. (13)] (b), and the flow rate correction Q_c [Eq. (7)] (c) as functions of α for $Ra_{uni} = 0$, $Ra_{P,L} = 250$, $A = 0.1$, and selected Ω 's. Dashed and dotted lines give reference results for the grooved isothermal and smooth periodically heated channels, respectively. Gray shading identifies α 's leading to a reduction of pressure losses in a grooved isothermal channel. Green lines mark $\alpha = 1$.

relative position of both patterns. The same conclusions can be reached on the basis of variations of ξ illustrated in Fig. 9(b). Variations of Q_c illustrated in Fig. 9(c) demonstrate a small increase of flow losses associated with addition of grooves for α 's in the RB zone for the best relative position of both patterns. Use of α 's in the drag-reducing zone shows reduction of flow losses when grooves are combined with periodic heating with the relative position of both patterns playing a minor role. It becomes obvious that use of $\alpha \approx 1$ produces the most intense streaks according to Figs. 9(a) and 9(b) but the energy cost is smaller than the maximum cost according to data in Fig. 9(c). The reader may recall that weak streaks produced by isothermal grooves are sufficient to produce chaotic stirring [22] which suggests that use of heating in combination with grooves should be a powerful technique for stirring intensification.

V. COMBINED PERIODIC AND UNIFORM HEATING

The final question to be addressed is the assessment of potential gains associated with combining the uniform and periodic heating of grooved surfaces. Use of α 's in the RB zone shows a rapid increase of ΔE_k as Ra_{uni} increases but the difference between heating of smooth and grooved surfaces is minor with a small preference for heating smooth surfaces at higher Ra'_{uni} 's [see Fig. 10(a)]. Use of $\alpha = 1$, which represents the optimal wave numbers, shows an advantage at small Ra'_{uni} 's but use of $\alpha = 1.57$ (the RB zone) is more effective at larger Ra'_{uni} 's. Use of $\alpha = 0.6$ (drag-reducing zone) produces much weaker streaks with a significant advantage for grooved surfaces in comparison to the smooth periodically heated channel. Use of ξ shows a similar pattern of variations [see Fig. 10(b)] with optimal α 's and α 's in the RB zone being equally competitive. The flow losses for the grooved and smooth surfaces are similar as shown in Fig. 10(c) and increase with Ra_{uni} . The advantage of using the optimal α is due to its ability to produce strong streaks at a much lower energy cost that increases with an increase of Ra_{uni} .

The reader should note that reduction of α leads to a reduction of flow losses [23] but its excessive reduction combined with an excessive heating leads to formation of secondary convection near the hot spots, which generates localized streaks [54,55]. Formation of such streaks was not of interest in this study.

VI. SUMMARY

The creation of streaks in low Reynolds number laminar shear flows is of interest for the intensification of stirring. This analysis is focused on the use of grooves for the intensification of

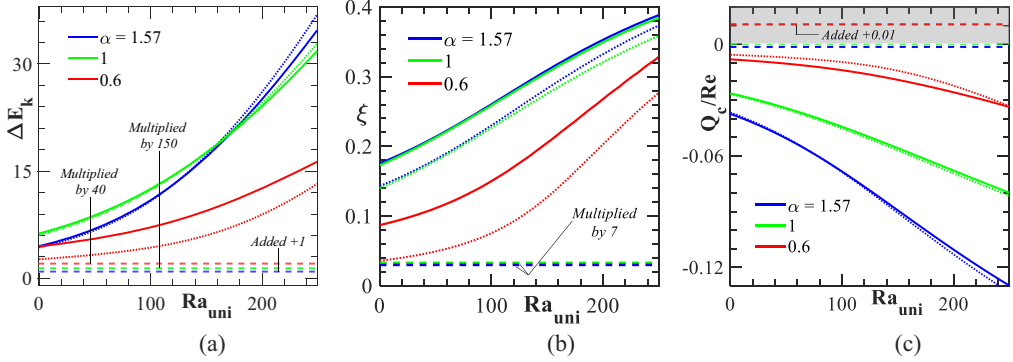


FIG. 10. Variations of the change in kinetic energy ΔE_k [Eq. (12)] (a), the maximum of the spanwise velocity gradient ξ [Eq. (13)] (b), and the flow rate correction Q_c [Eq. (7)] (c) as functions of Ra_{uni} for $A = 0.1$, $Ra_{P,L} = 250$, $\Omega = \pi/2$. Blue identifies $\alpha = 1.57$ (the RB zone), red identifies $\alpha = 0.6$ (the drag-reducing zone), and green identifies $\alpha = 1$. Dotted and dashed lines illustrate results for smooth periodically heated channels and for isothermal grooved channels, respectively. Gray shading in (c) identifies conditions leading to a reduction of flow losses.

streaks created by heating. Grooves play two roles: (i) they produce spanwise flow modulations which contribute to streak creation and (ii) they can reduce flow losses if their wavelength is long enough. Heating patterns applied to smooth surfaces are known to produce streaks. The combination of such heating and groove patterns leads to the formation of more intense streaks with smaller losses compared to heated smooth surfaces. The interest in this analysis was focused on low heating intensity and small groove amplitudes to control the energy “cost” associated with streak formation, and on heating patterns perfectly tuned with groove patterns.

The model problem involves pressure-gradient-driven channel flow with the lower wall fitted with streamwise grooves and exposed to a combination of uniform and spanwise-periodic heating with the spatial distribution matching the groove distribution. The model allows for different relative positions of the groove and heating patterns. The flow equations were solved numerically with spectral accuracy with geometry modeling carried out using the immersed boundary conditions concept which uses constraints equivalent to the imposition of boundary conditions at the borders of the flow domain. The efficiency of the streak creation was measured either by the pressure gradient correction when the fixed flow rate constraint was used or by the flow rate correction when the fixed pressure gradient constraint was used.

It is shown that isothermal grooves create relatively weak streaks. Uniform heating of these grooves results in the formation of intense streaks but only when the groove wave number is near the critical RB wave number and when the heating intensity either meets or exceeds the critical uniform Rayleigh number. The flow losses caused by such heating increase above the losses associated with isothermal grooves. The need to match the critical RB wave number limits the ability to create intense streaks with different spatial distributions. The need to match the critical heating intensity prevents the use of this method for streak creation using weak heating. The use of long-wavelength grooves reduces losses below those found in an isothermal smooth channel, but the resulting streaks have a much lower intensity. The streak intensity can be increased by increasing the groove amplitude.

Patterned heating of grooved surfaces demonstrates the potential for a significant increase of streak intensity as compared to patterned heating of smooth surfaces and uniform heating of grooved surfaces. It also provides the means for control of the spatial distributions of streaks and for the creation of such streaks using low-intensity heating. The strongest streaks are formed using $\alpha \approx 1$ with these streaks being stronger than streaks formed by the RB instability mechanism and having a much lower cost in terms of flow losses. Streaks formed by long-wavelength patterns remain

of interest as they have a respectable intensity but much lower energy cost. The relative position of both patterns plays an important role with the best effect obtained when hot spots are located approximately halfway between the groove crest and trough.

ACKNOWLEDGMENT

This work has been carried out with support from NSERC of Canada.

-
- [1] C. Eckart, An analysis of the stirring and mixing processes in incompressible fluids, *J. Mar. Res.* **7**, 265 (1948).
 - [2] J. M. Ottino, *The Kinematics of Mixing: Stretching, Chaos and Transport* (Cambridge University Press, Cambridge, UK, 1989).
 - [3] H. Yang, Chaotic mixing and transport in wave systems and the atmosphere, *Int. J. Bifurcation Chaos* **3**, 6 (1993).
 - [4] E. Villermaux, Mixing versus stirring, *Annu. Rev. Fluid Mech.* **51**, 245 (2019).
 - [5] A. E. Bergles, The implications and challenges of enhanced heat transfer for the chemical process industries, *Chem. Eng. Res. Des.* **79**, 4 (2001).
 - [6] P. M. Ligrani, M. M. Oliveira, and T. Blaskovich, Comparison of heat transfer augmentation techniques, *AIAA J.* **41**, 3 (2003).
 - [7] M. Siddique, A. R. A. Khaled, N. I. Abdulhafiz, and A. Y. Boukhary, Recent advances in heat transfer Enhancements: A review report, *Int. J. Chem. Eng.* **2010**, 106461 (2010).
 - [8] S. Balasuriya, Optimal Frequency for Microfluidic Mixing across a Fluid Interface, *Phys. Rev. Lett.* **105**, 064501 (2010).
 - [9] K. M. Butler and B. F. Farrell, Three-dimensional optimal perturbations in viscous shear flow, *Phys. Fluids A* **4**, 1637 (1992).
 - [10] F. Waleffe, On a self-sustaining process in shear flows, *Phys. Fluids* **9**, 883 (1997).
 - [11] F. Waleffe, Homotopy of exact coherent structures in plane shear flows, *Phys. Fluids* **15**, 1517 (2003).
 - [12] S. I. Chernyshenko and M. F. Baig, The mechanism of streak formation in near-wall turbulence, *J. Fluid Mech.* **544**, 99 (2005).
 - [13] J. Jiménez, How linear is wall-bounded turbulence?, *Phys. Fluids* **25**, 110814 (2013).
 - [14] J. Park, Y. Hwang, and C. Cossu, On the stability of large-scale streaks in turbulent Couette and Poiseuille flows, *C. R. Mec.* **339**, 1 (2011).
 - [15] K. E. Omari, E. Younes, T. Burghelca, C. Castelian, Y. Moguen, and Y. L. Guer, Active chaotic mixing in a channel with rotating arc-walls, *Phys. Rev. Fluids* **6**, 024502 (2021).
 - [16] J. M. Floryan, On the Görtler instability of boundary layers, *Prog. Aerospace Sci.* **28**, 235 (1991).
 - [17] P. J. Schmid and D. S. Henningson, *Stability and Transition in Shear Flows* (Springer, Berlin, Germany, 2001).
 - [18] A. E. Bergles, *Handbook of Heat Transfer*, 3rd ed. (McGraw-Hill, New York, US, 1998).
 - [19] S. Panday and J. M. Floryan, Creation of streaks using heating patterns, *Phys. Fluids* **33**, 083604 (2021).
 - [20] A. Mohammadi, H. V. Moradi, and J. M. Floryan, New instability mode in a grooved channel, *J. Fluid Mech.* **778**, 691 (2015).
 - [21] H. V. Moradi and J. M. Floryan, Stability of flow in a channel with longitudinal grooves, *J. Fluid Mech.* **757**, 613 (2014).
 - [22] S. W. Gepner and J. M. Floryan, Use of surface corrugations for energy-efficient chaotic stirring in low Reynolds number flows, *Sci. Rep.* **10**, 9865 (2020).
 - [23] A. Mohammadi and J. M. Floryan, Pressure losses in grooved channels, *J. Fluid Mech.* **725**, 23 (2013).
 - [24] M. Muthuramalingam, L. S. Villemin, and C. Brueckner, Streak formation in flow over biomimetic fish scale arrays, *J. Exp. Biol.* **222**, 205963 (2019).

- [25] A. D. Stroock, S. K. W. Dertinger, A. Ajdari, I. Mezic, H. A. Stone, and G. M. Whitesides, Chaotic mixer for microchannels, *Science* **295**, 647 (2002).
- [26] J. W. S. Rayleigh, On convection currents in a horizontal layer of fluid, when the higher temperature is on the under side, *Philos. Mag.* **32**, 529 (1916).
- [27] H. Bénard, Les tourbillons cellulaires dans une nappe liquide, *Rev. Gen. Sci. Pure Appl.* **11**, 1261 (1900).
- [28] R. E. Kelly, The onset and development of thermal convection in fully developed shear flows, *Adv. Appl. Mech.* **31**, 35 (1994).
- [29] M. Akiyama, G. J. Hwang, and K. C. Cheng, Experiments on the onset of longitudinal vortices in laminar forced convection between horizontal plates, *J. Heat Transfer* **93**, 335 (1971).
- [30] R. S. Wu and K. C. Cheng, Thermal instability of Blasius flow along horizontal plates, *Int. J. Heat Mass Transfer* **105**, 907 (1976).
- [31] A. Moutsoglou, T. S. Chen, and I. C. Cheng, Vortex instability of mixed convection flow over a horizontal flat plate, *J. Heat Transfer* **103**, 257 (1981).
- [32] K. Clien and M. M. Cheng, Thermal instability of forced convection boundary layers, *J. Heat Transfer* **106**, 284 (1984).
- [33] X. A. Wang, An experimental study of mixed forced and free convection heat transfer from a horizontal flat plate to air, *J. Heat Transfer* **104**, 139 (1982).
- [34] J. M. Floryan, Flow management using natural instabilities, *Arch. of Mech.* **58**, 575 (2006).
- [35] H. V. Moradi, A. C. Budiman, and J. M. Floryan, Use of natural instabilities for generation of streamwise vortices in a channel, *Theor. Comput. Fluid Dyn.* **31**, 233 (2017).
- [36] M. Z. Hossain and J. M. Floryan, Instabilities of natural convection in a periodically heated layer, *J. Fluid Mech.* **733**, 33 (2013).
- [37] M. Z. Hossain and J. M. Floryan, Mixed convection in a periodically heated channel, *J. Fluid Mech.* **768**, 51 (2015).
- [38] M. Z. Hossain and J. M. Floryan, Wavenumber lock-in and spatial parametric resonance in convection, *J. Fluid Mech.* **944**, A47 (2022).
- [39] M. Z. Hossain, D. Floryan, and J. M. Floryan, Drag reduction due to spatial thermal modulations, *J. Fluid Mech.* **713**, 398 (2012).
- [40] A. Inasawa, K. Taneda, and J. M. Floryan, Experiments on flows in channels with spatially distributed heating, *J. Fluid Mech.* **872**, 177 (2019).
- [41] J. M. Floryan, S. Shadman, and M. Z. Hossain, Heating-induced drag reduction in relative movement of parallel plates, *Phys. Rev. Fluids* **3**, 094101 (2018).
- [42] T. C. Jin, J. Z. Wu, Y. Z. Zhang, Y. L. Liu, and Q. Zhou, Shear-induced modulation of thermal convection over rough plates, *J. Fluid Mech.* **936**, A28 (2022).
- [43] S. Paolucci, *On the Filtering of Sound from the Navier-Stokes Equations*, Report No. SAND 82-8257 (Sandia National Laboratories, Livermore, CA, 1982).
- [44] J. Szumbariski and J. M. Floryan, A direct spectral method for determination of flows over corrugated boundaries, *J. Comput. Phys.* **153**, 378 (1999).
- [45] S. Z. Husain, J. Szumbariski, and J. M. Floryan, Over-constrained formulation of the immersed boundary condition method, *Comput. Methods Appl. Mech. Eng.* **199**, 94 (2009).
- [46] S. Z. Husain and J. M. Floryan, Spectrally-accurate algorithm for moving boundary problems for the Navier-Stokes equations, *J. Comput. Phys.* **229**, 2287 (2010).
- [47] A. Cabal, J. Szumbariski, and J. M. Floryan, Numerical simulation of flows over corrugated walls, *Comput. Fluids* **30**, 753 (2001).
- [48] S. Panday and J. M. Floryan, An algorithm for analysis of pressure losses in heated channels, *Int. J. Numer. Methods Fluids* **93**, 1332 (2021).
- [49] Y. Chen, J. M. Floryan, Y. T. Chew, and B. C. Khoo, Groove-induced changes of discharge in channel flows, *J. Fluid Mech.* **799**, 297 (2016).
- [50] A. Abtahi and J. M. Floryan, Natural convection in corrugated slots, *J. Fluid Mech.* **815**, 537 (2017).
- [51] A. Abtahi and J. M. Floryan, Natural convection and thermal drift, *J. Fluid Mech.* **826**, 553 (2017).
- [52] J. M. Floryan and A. Inasawa, Pattern interaction effect, *Sci. Rep.* **11**, 14573 (2021).
- [53] A. Abtahi and J. M. Floryan, On the formation of thermal drift, *Phys. Fluids* **30**, 043602 (2018).

- [54] A. Asgarian, M. Z. Hossain, and J. M. Floryan, Rayleigh–Bénard convection driven by a long wavelength heating, [Theor. Comput Fluid Dyn.](#) **30**, 313 (2016).
- [55] J. M. Floryan, M. Z. Hossain, and A. P. Bassom, Modified Rayleigh–Bénard convection driven by long-wavelength heating from above and below, [Theor. Comput. Fluid Dyn.](#) **33**, 37 (2019).